Calculation of the ion velocity distribution function in a rotating plasma

Jørgensen, L.W.

Publication date:
1978

Document Version
Publisher's PDF, also known as Version of record

Risø Report No. 384

Risø Report No. 384

Risø National Laboratory

Calculation of the Ion Velocity Distribution Function in a Rotating Plasma

by L. W. Jørgensen

October 1978

Sales distributors: Jul. Gjellerup, Sølvgade 87, DK-1307 Copenhagen K, Denmark

Available on exchange from: Risø Library, Risø National Laboratory, P O. Box 49, DK-4000 Roskilde, Denmark

Risø Report No. 384

CALCULATION OF THE ION VELOCITY DISTRIBUTION FUNCTION IN A ROTATING PLASMA[+]

L.W. Jørgensen[*]

Association Euratom - Risø
Risø National Laboratory
Physics Department
DK-4000 Roskilde

ABSTRACT

Using a single-particle orbit picture of the plasma ions in the puffatron (a device with rotating plasma), the corresponding ion velocity distribution function is calculated. The spread in the ion Larmor velocity due to the initial break-down phase is taken into account assuming a parabolic distribution for this spread. The calculated ion velocity distribution function is integrated along a chord in order to make it possible to compare the calculations with suitable measurements along a chord of the ion velocity spectrum.

UDC 533.9

[+] This work was supported by the Danish Natural Science Research Council

[*] Present address: Culham Laboratory, Abingdon Oxfordshire OX14 3DB, United Kingdom.

ISBN 87-550-0563-2
ISSN 0418-6443

CONTENTS

1. INTRODUCTION

There is interest in cross-field discharges with strong electric and magnetic fields from many different points of view. Lehnert (1971) gave a review of this configuration in which the basic idea is a radial electric field and a longitudinal magnetic field where the plasma is created, heated, and forced to rotate.

Besides the possibilities for creating and containing very hot ion plasmas for the purpose of fusion reactions, rotating plasmas have been examined with a view to element and isotope separation, including plasma impurities, because of the centrifugal force (Bonnevier, 1971) (James and Simpson, 1974). Srnka (1974) used a rotating plasma in a solar wind simulation experiment. We used our rotating plasma for several years in a study of the interaction between a hydrogen pellet and a plasma with the refuelling of fusion reactors in mind (Jørgensen et al., 1977) (Jørgensen and Sillesen, 1978).

A schematic outline of the puffatron device is shown in fig. 1. The discharge chamber is in principle a cylinder condenser (with the voltage between the concentric electrodes at 5-50 kV) parallel with the axial magnetic field (field strength up to 1.5 T), which has a 60 cm long uniform section symmetrically around the midplane of the machine and a mirror ratio of 1.5. Outer electrode, r_y = 7.5 cm and inner electrode, r_i = 2.5 cm. The filling gas for a discharge is puffed into the vacuum chamber from a small gas chamber at the center of the inner electrode through a fast acting valve. After introduction of the gas, which spreads radially and axially in the vacuum chamber, the electric field is switched on. This results in a very short break-down phase of a few μs (Bonnevier and Sillesen, 1974) and a fully ionized plasma with initial densities at 10^{14} - 10^{15} cm^{-3} depending on the filling pressure of the gas chamber (Rasmussen et al., 1978). By introducing the filling

gas in this way, we avoid critical velocity phenomena of the ions (Danielson, 1970) and break-down over insulators. For further experimental details and measurements, see Øster (1969).

Since a plasma model based on single-particle orbit theory has been able to explain several plasma phenomena in this type of plasmas,we have used this model in a calculation of the ion velocity distribution.

2. THE PLASMA MODEL

As mentioned in the introduction, single-particle orbit theory was used for the ions. The equation of motion for a charged particle created in an electric field $\underline{E}$ and a magnetic field $\underline{B}$ is

$$m \frac{d\underline{v}}{dt} = e(\underline{E} + \underline{v} \times \underline{B} \tag{1}$$

where m, e and $\underline{v}$ are, respectively, the mass, the electric charge and the velocity of the particle. Figure 2 shows a schematic cross-section of the puffatron device. For the electric field, we have

$$E(r) = \frac{V}{r \ln \frac{r_y}{r_i}} \tag{2}$$

where V is the voltage between the inner and the outer electrode.

An analytic solution of equation (1) seems impossible in our cylindrical geometry. In a system with plane parallel electrodes, the solution to equation (1) is cycloids with a radius equal to the Larmor radius

$$r_{L_{i,e}} = \frac{v_D}{\omega_{c_{i,e}}} = \frac{m_{i,e} E}{e B^2} \tag{3}$$

where v_D is the drift velocity

$$v_{D_{i,e}} = \frac{E}{B} \tag{4}$$

and ω_c is the Larmor frequency

$$\omega_{c_{i,e}} = \frac{\pm e B}{m_{i,e}} . \tag{5}$$

Øster (1969) showed that in the cylindrical case the orbit can be approximated to these cycloids with a cricle as base, see fig. 2. Appendix 1 contains a numerical calculation of the actual orbit, which is compared with the cycloidal orbit. It is seen that the above approximation is good.

Until now we have assumed that the E-field is time-independent, but as the E-field is determined by the voltage between the electrodes, equation (2), this assumption is not fulfilled. However, the E-field changes slowly in relation to a Larmor period, so $v_D(t)$ is determined by $E(t)$, while the Larmor velocity is determined by $v_L(t) = v_D(t_o)$, where t_o is the time at which the charged particle was ionized. Therefore it is not possible to change the Larmor velocity externally after the creation time.

3. THE ION VELOCITY DISTRIBUTION FUNCTION

In these calculations the simple theory from chapter 2 is applied and this means that the ion velocity is always perpendicular to the magnetic field, fig. 3. In order to calculate the ion velocity distribution function, $f(v_x)$ in an arbitrary direction we need to know the Larmor velocity distribution function, $f(v_L)$, but this demands detailed knowledge of the ionization phase. In the following we will assume that $f(v_L)$ can be approximated to a parabola, fig. 4.

It may be assumed that the creation of plasma particles in the breakdown process occurs randomly in time so that the phases of the Larmor velocity vectors are uncorrelated, which means that

$$f(\underline{v}_L) = \frac{f(v_L)}{2\pi\, v_L}$$

$$= \begin{cases} \dfrac{3}{8\pi b}\, \dfrac{1 - \frac{1}{b^2}\left(\sqrt{v_{L_x}^2 + v_{L_y}^2} - v_L'\right)^2}{\sqrt{v_{L_x}^2 + v_{L_y}^2}} & \text{for } v_L' - b \leq \sqrt{v_{L_x}^2 + v_{L_y}^2} \leq v_L' + b \\ 0 \text{ elsewhere} & \end{cases} \tag{6}$$

and

$$f(v_{L_x}) = \int_{-\infty}^{\infty} f(v_{L_x}, v_{L_y})\, dv_{L_y}. \tag{7}$$

From equations (6), (7) and the identity

$$f(v_x) = f(v_{L_x}) \left.\frac{dv_{L_x}}{dv_x}\right|_{v_{L_x} = v_x - v_{D_x}}$$

we find

$$f(u) = \frac{3}{8\pi\beta^3}\begin{cases} (3\alpha-\beta)\sqrt{(\alpha+\beta)^2-(u-1)^2}-(3\alpha+\beta)\sqrt{(\alpha-\beta)^2-(u-1)^2} \\ \quad +(2\beta^2-2\alpha^2-(u-1)^2)\ln\dfrac{\alpha+\beta+\sqrt{(\alpha+\beta)^2-(u-1)^2}}{\alpha-\beta+\sqrt{(\alpha-\beta)^2-(u-1)^2}} \\ \quad \text{for } 1-(\alpha-\beta)\le u \le 1+\alpha-\beta \\ (3\alpha-\beta)\sqrt{(\alpha+\beta)^2-(u-1)^2}+\frac{1}{2}(2\beta^2-2\alpha^2-(u-1)^2)\times \\ \quad \ln\dfrac{\alpha+\beta+\sqrt{(\alpha+\beta)^2-(u-1)^2}}{\alpha+\beta-\sqrt{(\alpha+\beta)^2-(u-1)^2}} \\ \quad \text{for } (1-(\alpha+\beta)\le u \le 1-(\alpha-\beta))\,\mathrm{v}\,(1+\alpha-\beta\le u\le 1+\alpha+\beta) \\ 0 \text{ elsewhere} \end{cases} \tag{8}$$

where

$$u \equiv \frac{v_x}{v_{D_x}},\quad \alpha \equiv \frac{v_L}{v_{D_x}},\quad \beta \equiv \frac{b}{v_{D_x}} \tag{9}$$

and we have assumed that $\beta < \alpha$. For convenience, the stroke on v_L is omitted.

If we approximate $f(v_L)$ with a δ-function, we can find the corresponding function, $f_\delta(u)$ to $f(u)$, by

$$f_\delta(u) = \lim_{\beta\to 0} f(u) = \begin{cases} \dfrac{1}{\pi}\dfrac{1}{\sqrt{\alpha^2-(u-1)^2}} & \text{for } 1-\alpha<u<1+\alpha \\ 0 \text{ elsewhere} \end{cases} \tag{10}$$

where we use L'Hospital's theorem. $f(u)$ and $f_\delta(u)$ are shown for several values of α and β on fig. 5.

4. THE ION VELOCITY DISTRIBUTION FUNCTION INTEGRATED ALONG A CHORD

The integration path and nomenclature are shown on fig. 6. We have

$$d\Omega = \frac{r d\phi}{\sin\phi} = \frac{a}{\sin^2\phi}\, d\phi, \tag{11}$$

and

$$\begin{aligned}
v_D &= v_D(r) = v_D(a)\sin\phi = v_{D_o}\sin\phi \quad \text{where } v_{D_o} \equiv v_D(a) \\
v_L &= v_L(r) = v_L(a)\sin\phi = v_{L_o}\sin\phi \quad \text{where } v_{L_o} \equiv v_L(a) \\
u &= \frac{v_x}{v_{D_x}} = \frac{v_x}{v_{D_o}\sin^2\phi} = \frac{u_o}{\sin^2\phi} \quad \text{where } u_o \equiv \frac{v_x}{v_{D_o}} \\
\alpha &= \frac{v_L}{v_{D_x}} = \frac{v_{L_o}\sin\phi}{v_{D_o}\sin^2\phi} = \frac{\alpha_o}{\sin\phi} \quad \text{where } \alpha_o \equiv \frac{v_{L_o}}{v_{D_o}} \\
\beta &= \frac{b}{v_{D_x}} = \frac{b_o\sin\phi}{v_{D_o}\sin\phi} = \beta_o \quad \text{where } \beta_o \equiv \beta(a)
\end{aligned} \tag{12}$$

This means that the relations

$$\frac{v_L(r)}{v_D(r)} = \frac{v_{L_o}}{v_{D_o}} = \alpha_o \quad \text{and} \quad \frac{b(r)}{v_L(r)} = \frac{\beta_o}{\alpha_o} \tag{13}$$

are assumed to be independent of the position on the chord. Now, the integrated ion velocity distribution function is

$$g(v_x) = \int_{\phi_1}^{\pi-\phi_1} n\, f(v_x,\phi)\, d\Omega = 2a \int_{\phi_1}^{\frac{\pi}{2}} n\, f(v_x,\phi)\frac{d\phi}{\sin^2\phi} \tag{14}$$

where n is the number density of the plasma ions. Here we use the fact that $f(v_x,\phi)/\sin^2\phi$ is symmetric around $\phi = \frac{\pi}{2}$, and it is temporarily assumed that n is constant along the chord.

4.1. $g(v_x)$ for a δ-function distribution for the Lamor velocity

In order to calculate equation (14) analytically, we will have to analyze the interval in equation (10)

$$1 - \alpha < u < 1 + \alpha$$

or, by using equation (12),

$$\sin^2\phi - \alpha_o\sin\phi < u_o < \sin^2\phi + \alpha_o\sin\phi. \qquad (15)$$

Equation (14) is calculated in appendix 2 and it appears that there are five fundamentally different results depending on the value of α_o: $0 \le \alpha_o \le 1-\sin\phi_1$, $1-\sin\phi_1 \le \alpha_o \le 2\sin\phi_1$, $2\sin\phi_1 \le \alpha_o \le 1+\sin\phi_1$, $1+\sin\phi_1 \le \alpha_o \le 2$, and $2 \le \alpha_o$. Figure 7 shows $g(u_o)$ for representative values of α_o.

4.2. $g(v_x)$ for a parabolic function distribution for the Larmor velocity

In this case, a numerical calculation is made of equation (14). For further details see chapter 5. Figure 8 shows the result for $\alpha_o = 1$ and for different values of β_o. For $\beta_o = 0$, this case corresponds to the case in section 4.1. It is seen that for increasing values of β_o, $g(u_o)$ does not change essentially except for some smoothing out.

5. THE INFLUENCE OF PLASMA DENSITY GRADIENTS

In the previous chapter the plasma density was assumed to be constant in space. Nevertheless, this is not correct (Øster, 1969) (Rasmussen et al., 1978), because of the puff-valve system. We assume the neutral gas to have a radial density dependence proportional to r^{-q}, $2 < q < 3$. The discharge will take place when the neutral gas is spread out close to the outer electrode, and the ion density is expected to be proportional to the neutral density (Rasmussen et al.). Figure 9 shows $g(u_o)$ for $n(r) \sim r^{-q}$, calculated from equation (14). For the case of uniform plasma density, $g(u_o)$ is given by the curve of $q = 0$, and for $n(r) \sim r^{-3}$ decrease in density, $q(u_o)$ is shown by the curve of $q = 3$. Since it is our intention to measure the Doppler profile of the He II line in a helium plasma (Jørgensen and Sillesen,1978) we have also shown the curves of $q = 4$ and $q = 6$, which illustrate the Doppler profiles to be measured for $n(r) \sim r^{-2}$ and $n(r) \sim r^{-3}$, respectively, because the density of excited He II ions is proportional to the product of the ion density and the electron density, assuming that the electron temperature is constant along the chord.

The numerical calculations in this chapter and in chapter 4 are based on a Romberg quadrature procedure. The single points are determined with an error of less than 1%. The profiles in section 4.1 are obtained using a sufficiently small value of β_o, knowing that $g(u_o)$ is infinite in the α_o values determining the u_o intervals in appendix 2. In order to check the calculations, we made a planimeter integration of the single profiles that should result in the length of the chord, which it did within an error of less than 5%.

6. CONCLUSIONS

Based on a single-particle orbit model of the rotating plasma, we calculated the ion velocity distribution function $f(u; \alpha, \beta)$, where α is the ratio of the mean Larmor velocity to the drift velocity and β is a measure of the spreading in the Larmor velocity. In order to make it possible to verify the above plasma model by measurements of the ion velocity spectrum, we have also integrated $f(u; \alpha, \beta)$ along a chord in the plasma. In this integration the influence of plasma density gradients is also taken into account.

ACKNOWLEDGEMENT

The author is indebted to Dr. A.H. Sillesen for many valuable discussions and for suggesting improvements to this manuscript.

REFERENCES

BONNEVIER, B. (1971). Plasma Phys. 13, 763.

BONNEVIER, B. and SILLESEN, A.H. (1974). Breakdown and plasma formation in a rotating plasma device. Trit-EPP-74-06.

DANIELSSON, L. (1970). Physics Fluids 13, 2288.

JAMES, B.W. and SIMPSON, S.W. (1974). Phys. Lett. 46A, 347.

JØRGENSEN, L.W. and SILLESEN, A.H. (1978). Plasma Physics, to be published.

JØRGENSEN, L.W. and SILLESEN, A.H. (1978). Submitted to Plasma Physics.

JØRGENSEN, L.W., SILLESEN, A.H. and ØSTER, F. (1977). Plasma Phys. 19, 1093.

LEHNERT, B. (1971). Nucl. Fusion 11, 485.

ØSTER, F. (1969). Studies of a Rotating Plasma Device. Risø Report No. 191.

RASMUSSEN, O., SILLESEN, A.H. and WEISBERG, K.-W. (1978). Private.

SRNKA, L.J. (1974). Plasma Phys. 16, 1129.

APPENDIX 1

The orbit of a charged particle in cylindrical geometry

Rewriting equation (1) for a cylindrical coordinate system with z = 0 corresponding to the midplane of the puffatron device, we find

$$\ddot{r} - r\dot{\phi}^2 = \frac{\gamma_{i,e}}{r} - \omega_{c_{i,e}}$$

$$r\ddot{\phi} + 2\dot{r}\dot{\phi} = \omega_{i,e}\dot{r} \qquad (16)$$

with

$$\gamma_{i,e} \equiv \pm \frac{e\,V}{m_{i,e}\,\ln \frac{r_y}{r_i}}$$

where we use equations (2) and (5).

The speed of the charged particle is easily obtained from

$$\frac{1}{2}\,m\,v^2 = e\int_{r_o}^{r} E\,dr \qquad (17)$$

or using equation (2)

$$v_{i,e}^2 = 2\gamma_{i,e}\,\ln\frac{r}{r_o} \qquad (18)$$

where we assume that the charged particle starts with zero velocity at $r = r_o$.

An analytic solution of equation (16) seems impossible but, putting $\dot{r} = \psi$ and $\dot{\phi} = \zeta$, we find from equation (16) four coupled ordinary differential equations in r, ϕ, ψ and ζ. These are easily solved numerically with a standard procedure. In fig. 10 the results of these numerical calculations are shown for different values of (V,B) for a helium ion. In order to compare these orbits with cycloids, the length of $2r_L$ calculated from equation (3) is shown. In table 1 we have also compared the computed mean drift velocity and the cycle time with the drift velocity from equation (4) and $2\pi/\omega$ from equation (5), respectively. From fig. 10 and table 1 it is seen that the plane geometry approximation is good, especially for smaller electric fields and larger magnetic fields.

V	B	mean drift velocity	v_D	cycle time	$\frac{2\pi}{\omega}$
kV	T	$\times 10^5$ m/s	$\times 10^5$ m/s	ns	ns
25	1.5	2.48	3.03	200	175
15	1.5	1.62	1.82	191	175
5	1.5	0.59	0.61	181	175
5	.75	1.04	1.21	392	350

Table 1. The computed mean drift velocity and cycle time for a helium ion in a cylindrical geometry compared with v_D and $2\pi/\omega$ for a cycloid (equations (4) and (5)), for different values of V and B.

APPENDIX 2

The ion velocity distribution function integrated along a chord $g(v_x)$ assuming that all the ions have equal Larmor speed at the same position

This appendix shows the result of the tedious, but easy calculation of equation (14).

$2 \leq \alpha_o$:

$$g(u_o) = \begin{cases} 0 & \text{for } \alpha_o + 1 \leq u_o \\ \int_{\sin^{-1}(\ell_1)}^{\frac{\pi}{2}} K(u_o,\phi)\,d\phi & (\alpha_o+\sin\phi_1)\sin\phi_1 \leq u_o \leq \alpha_o+1 \\ \int_{\phi_1}^{\frac{\pi}{2}} K(u_o,\phi)\,d\phi & -(\alpha_o-\sin\phi_1)\sin\phi_1 \leq u_o \leq (\alpha_o+\sin\phi_1)\sin\phi_1 \\ \int_{-\sin^{-1}(\ell_1)}^{\frac{\pi}{2}} K(u_o,\phi)\,d\phi & -(\frac{\alpha_o}{2})^2 \leq u_o \leq -(\alpha_o-\sin\phi_1)\sin\phi_1 \\ 0 & u_o \leq -(\frac{\alpha_o}{2})^2 \end{cases}$$

$1 + \sin\phi_1 \le \alpha_o \le 2$:

$$g(u_o) = \begin{cases} 0 & \text{for } \alpha_o + 1 \le u_o \\ \int_{\sin^{-1}(\ell_1)}^{\frac{\pi}{2}} K(u_o,\phi)\,d\phi & (\alpha_o+\sin\phi_1)\sin\phi_1 \le u_o \le \alpha_o+1 \\ \int_{\phi_1}^{\frac{\pi}{2}} K(u_o,\phi)\,d\phi & -(\alpha_o-\sin\phi_1)\sin\phi_1 \le u_o \le (\alpha_o+\sin\phi_1)\sin\phi_1 \\ \int_{-\sin^{-1}(\ell_1)}^{\frac{\pi}{2}} K(u_o,\phi)\,d\phi & -(\alpha_o-1) \le u_o \le -(\alpha_o-\sin\phi_1)\sin\phi_1 \\ \int_{-\sin^{-1}(\ell_1)}^{\sin^{-1}(\ell_2)} K(u_o,\phi)\,d\phi & -(\frac{\alpha_o}{2})^2 \le u_o \le -(\alpha_o-1) \\ 0 & u_o \le -(\frac{\alpha_o}{2})^2 \end{cases}$$

$2\sin\phi_1 \le \alpha_o \le 1 + \sin\phi_1$:

$$g(u_o) = \begin{cases} 0 & \text{for } \alpha_o + 1 \le u_o \\ \int_{\sin^{-1}(\ell_1)}^{\frac{\pi}{2}} K(u_o,\phi)\,d\phi & (\alpha_o+\sin\phi_1)\sin\phi_1 \le u_o \le \alpha_o+1 \\ \int_{\phi_1}^{\frac{\pi}{2}} K(u_o,\phi)\,d\phi & -(\alpha_o-1) \le u_o \le (\alpha_o+\sin\phi_1)\sin\phi_1 \\ \int_{\phi_1}^{\sin^{-1}(\ell_2)} K(u_o,\phi)\,d\phi & -(\alpha_o-\sin\phi_1)\sin\phi_1 \le u_o \le -(\alpha_o-1) \\ \int_{-\sin^{-1}(\ell_1)}^{\sin^{-1}(\ell_2)} K(u_o,\phi)\,d\phi & -(\frac{\alpha_o}{2})^2 \le u_o \le -(\alpha_o-\sin\phi_1)\sin\phi_1 \\ 0 & u_o \le -(\frac{\alpha_o}{2})^2 \end{cases}$$

$1 - \sin\phi_1 \le \alpha_o \le 2\sin\phi_1$:

$$g(u_o) = \begin{cases} 0 & \text{for } \alpha_o + 1 \le u_o \\ \displaystyle\int_{\sin^{-1}(\ell_1)}^{\frac{\pi}{2}} K(u_o,\phi)\,d\phi & (\alpha_o+\sin\phi_1)\sin\phi_1 \le u_o \le \alpha_o+1 \\ \displaystyle\int_{\phi_1}^{\frac{\pi}{2}} K(u_o,\phi)\,d\phi & 1-\alpha_o \le u_o \le (\alpha_o+\sin\phi_1)\sin\phi_1 \\ \displaystyle\int_{\phi_1}^{\sin^{-1}(\ell_2)} K(u_o,\phi)\,d\phi & -(\alpha_o-\sin\phi_1)\sin\phi_1 \le u_o \le 1-\alpha_o \\ 0 & u_o \le -(\alpha_o - \sin\phi_1)\sin\phi_1 \end{cases}$$

$0 \le \alpha_o \le 1 - \sin\phi_1$:

$$g(u_o) = \begin{cases} 0 & \text{for } 1 + \alpha_o \le u_o \\ \displaystyle\int_{\sin^{-1}(\ell_1)}^{\frac{\pi}{2}} K(u_o,\phi)\,d\phi & 1 - \alpha_o \le u_o \le 1 + \alpha_o \\ \displaystyle\int_{\sin^{-1}(\ell_1)}^{\sin^{-1}(\ell_2)} K(u_o,\phi)\,d\phi & (\alpha_o + \sin\phi_1)\sin\phi_1 \le u_o \le 1-\alpha_o \\ \displaystyle\int_{\phi_1}^{\sin^{-1}(\ell_2)} K(u_o,\phi)\,d\phi & (\sin\phi_1-\alpha_o)\sin\phi_1 \le u_o \le (\alpha_o+\sin\phi_1)\sin\phi_1 \\ 0 & u_o \le (\sin\phi_1 - \alpha_o)\sin\phi_1 \end{cases}$$

where

$$K(u_o,\phi) = \frac{2\,n\,a}{\pi}\,\frac{1}{\sqrt{\alpha_o^2\sin^2\phi-(u_o-\sin^2\phi)^2}}\,\frac{1}{\sin^2\phi}$$

$$\ell_1 \equiv \frac{-\alpha_o + \sqrt{\alpha_o^2 + 4u_o}}{2}$$

$$\ell_2 \equiv \frac{\alpha_o + \sqrt{\alpha_o^2 + 4u_o}}{2}$$

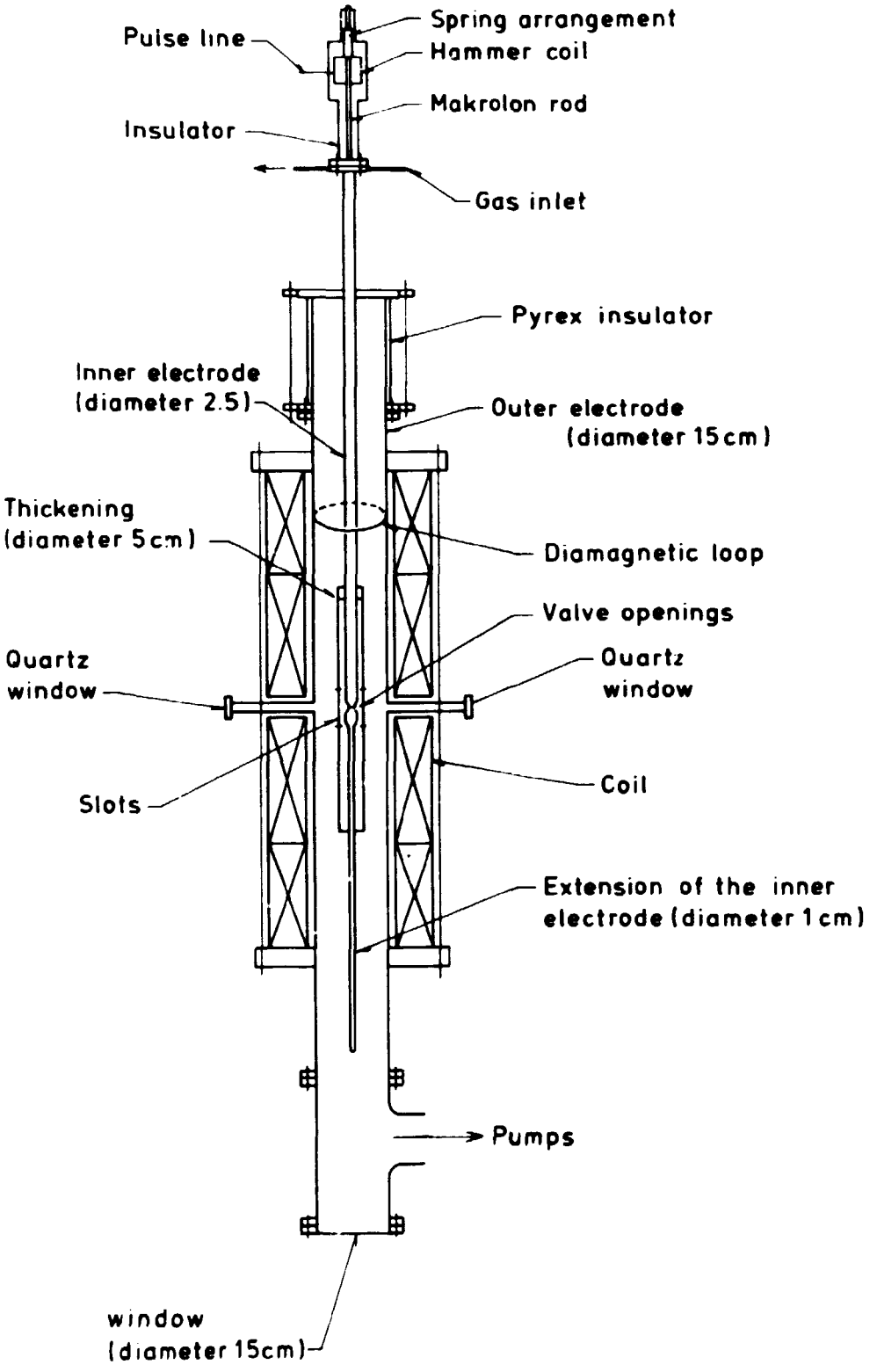

Fig. 1. Schematic diagram showing the puffatron device.

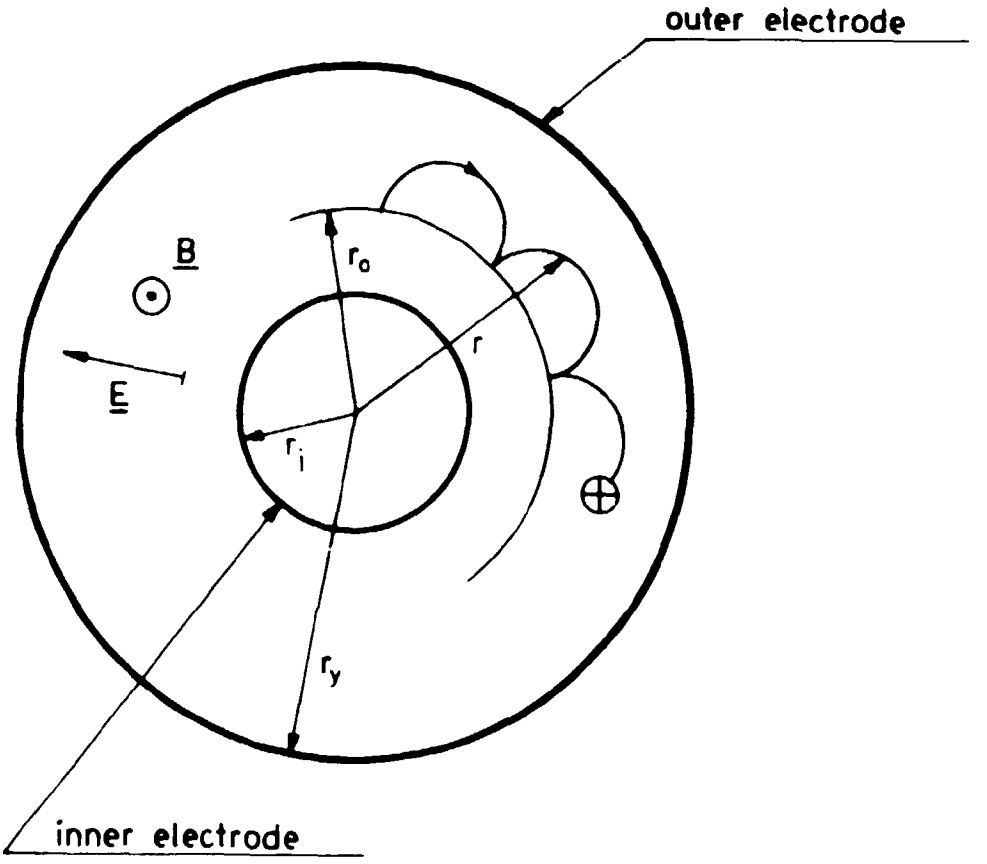

Fig. 2. A schematic diagram of the cross section of the puffatron device. A part of a characteristic ion orbit is also shown.

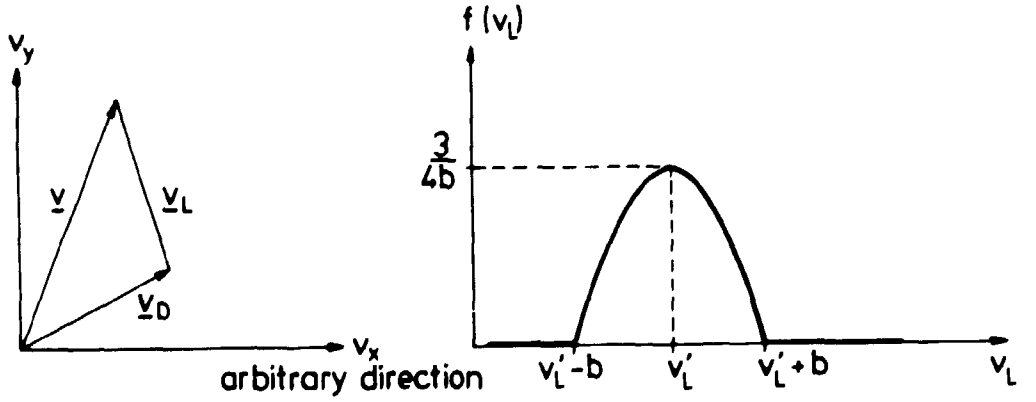

Fig. 3. The ion velocity, $\underline{v}$, composed of the Larmor velocity, $\underline{v}_L$, and the drift velocity, $\underline{v}_D$.

Fig. 4. The normalized Larmor velocity distribution, $f(v_L) = \frac{3}{4b}\left(1 - \frac{1}{b^2}(v_L - v_L')^2\right)$ for $v_L' - b \leq v_L \leq v_L' + b$, and equal to zero elsewhere.

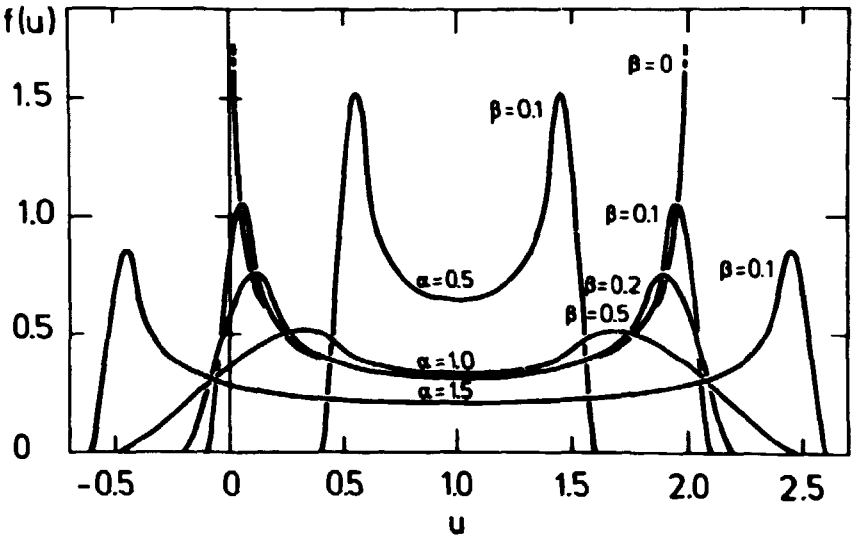

Fig. 5. The function f(u) for different values of α and β. For $\beta = 0$, we find $f(u) = f_{\delta}(u)$.

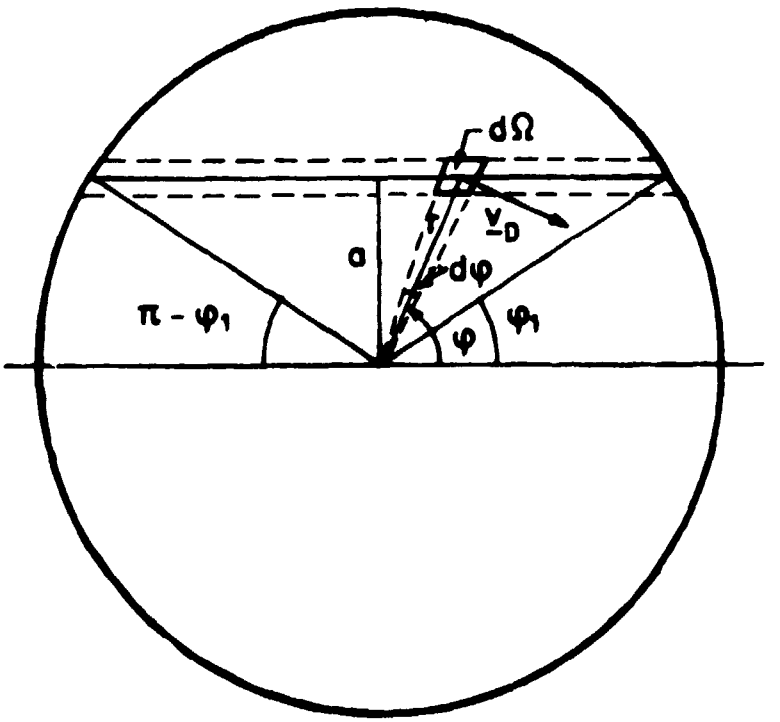

Fig. 6. A schematic diagram of the cross section of the puffatron device showing the chord along which the integration is performed.

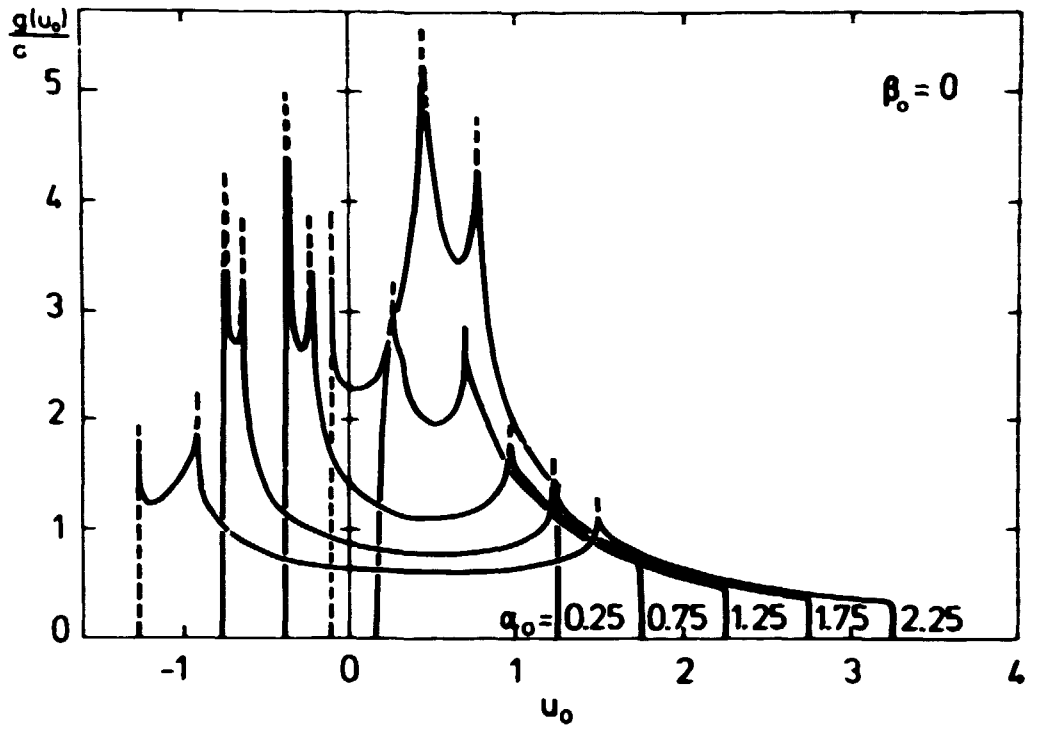

Fig. 7. The function $g(u_o)$ for different values of α_o for β_o=0.

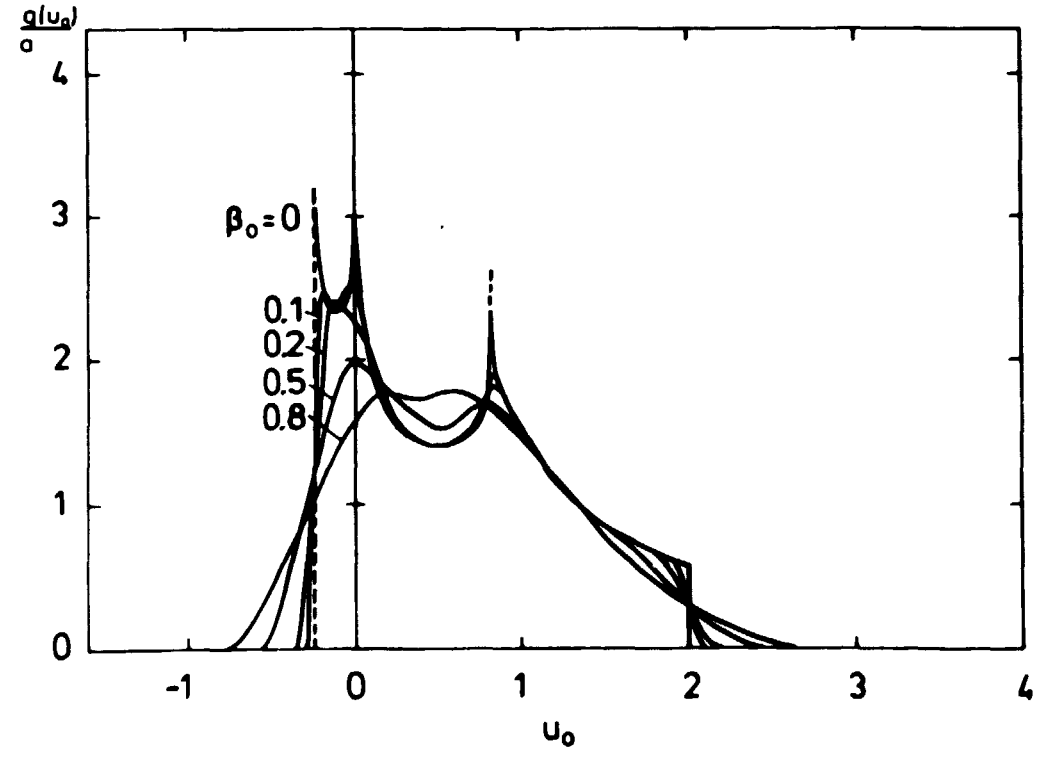

Fig. 8. The function $g(u_o)$ for α_o = 1 and different values of β_o.

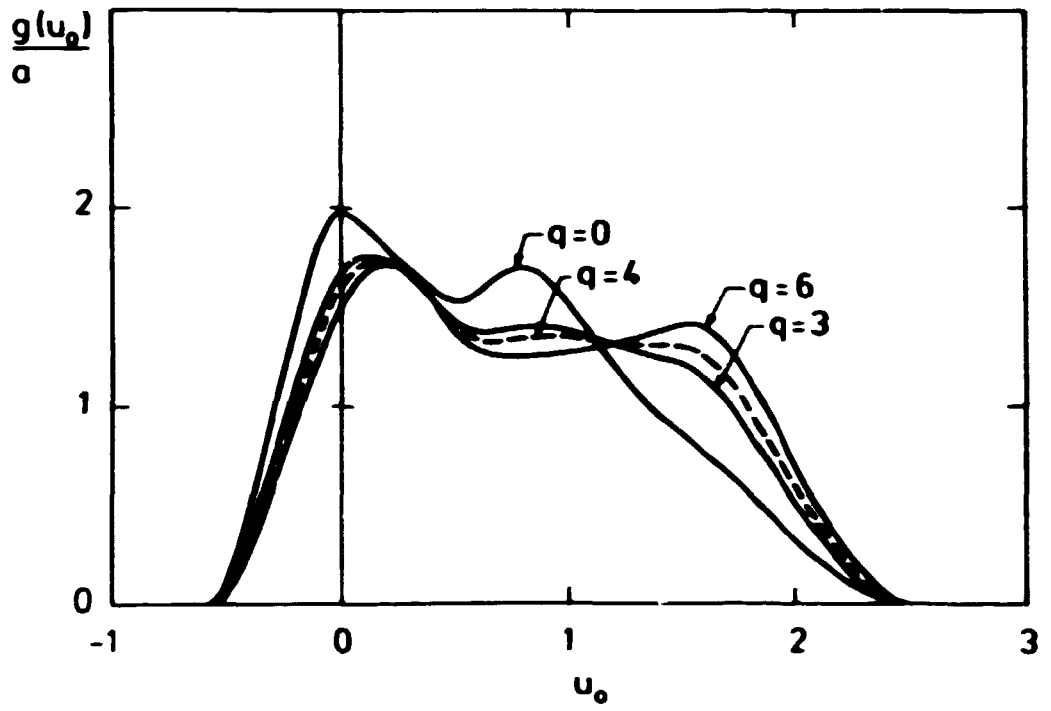

Fig. 9. The function $g(u_o)$ for $\alpha_o = 1$, $\beta_o = 0.5$ with different density profiles, $n(r) \sim 1/r^q$, $q = 0$, 3, 4 and 6.

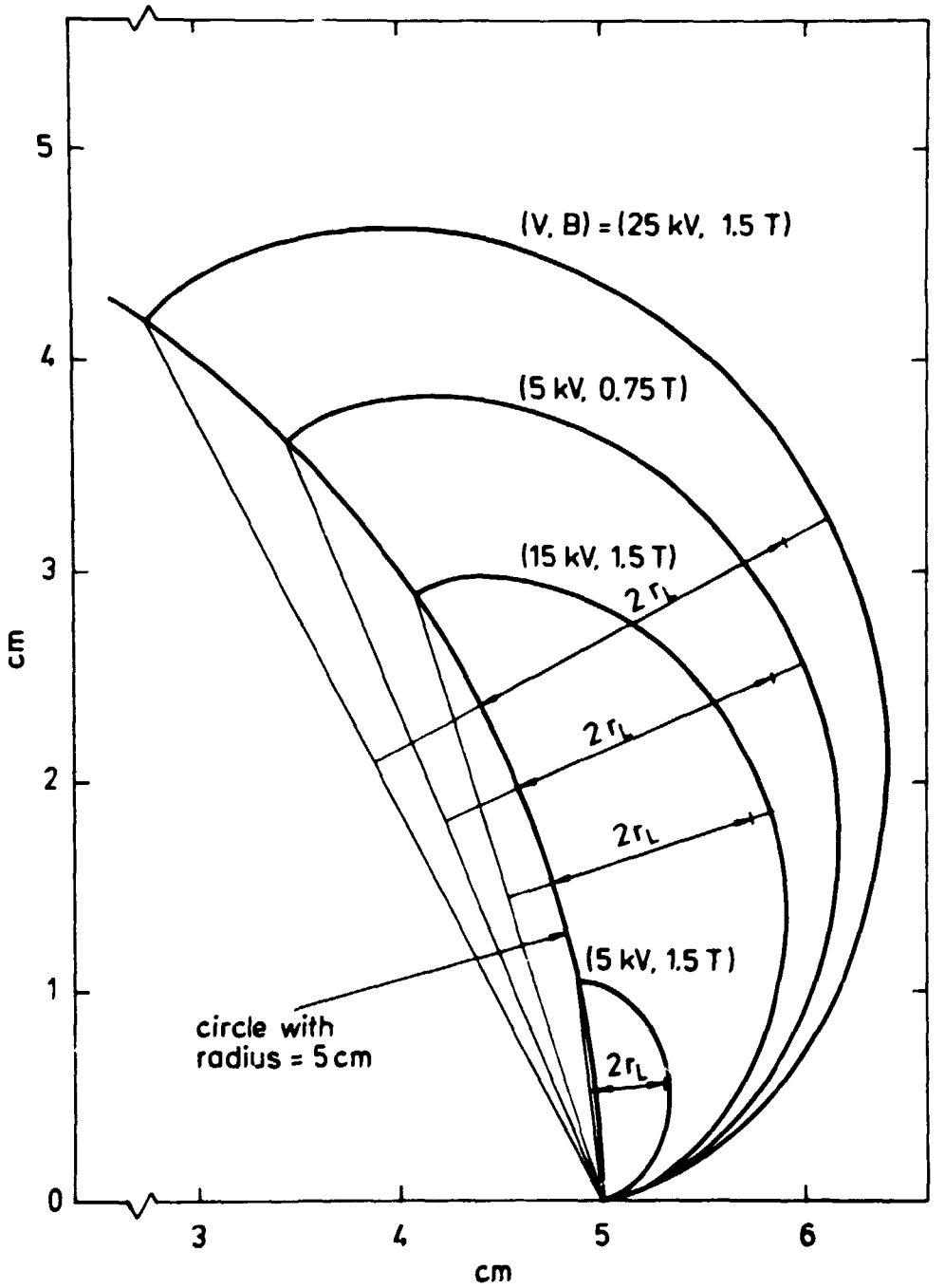

Fig. 10. The computed helium ion orbit in a cylindrical geometry for different values of V and B. In order to compare with cycloids, $2r_L$, from equation (3), is shown.

ISBN 87-550-0563-2
ISSN 0418-6443